

Fingerprints of the initial conditions on the density profiles of cold and warm dark matter haloes

E. Polisensky^{1*} and M. Ricotti^{2*†}

¹*Naval Research Laboratory, Washington, D.C. 20375, USA*

²*Department of Astronomy, University of Maryland, College Park, Maryland 20745, USA*

16 March 2021

ABSTRACT

We use N-body simulations of dark matter haloes in cold dark matter (CDM) and a large set of different warm dark matter (WDM) cosmologies to demonstrate that the spherically averaged density profile of dark matter haloes has a shape that depends on the power spectrum of matter perturbations. Density profiles are steeper in WDM but become shallower at $r < 0.01R_{vir}$. Virialization isotropizes the velocity dispersion in the inner regions of the halo but does not erase the memory of the initial conditions in phase space. The location of the observed deviations from CDM in the density profile and in phase space can be directly related to the ratio between the halo mass and the filtering mass and are most evident in small mass haloes, even for a 34 keV thermal relic WDM. The rearrangement of mass within the haloes supports analytic models of halo structure that include angular momentum. We also find evidence of a dependence of the slope of the inner density profile in CDM cosmologies on the halo mass with more massive haloes exhibiting steeper profiles, in agreement with the model predictions and with previous simulation results. Our work complements recent studies of microhaloes near the filtering scale in CDM and strongly argue against a universal shape for the density profile.

Key words: galaxies: haloes, dwarf, cosmology: theory, dark matter

1 INTRODUCTION

The seminal work of Navarro et al. (1996) found that the density structure of relaxed dark matter haloes are well represented by what has become known as the NFW profile:

$$\rho(r) = \frac{\rho_s}{(r/r_s)(1+r/r_s)^2}, \quad (1)$$

where $\rho(r)$ is the density in a spherical shell at distance r from the halo centre. By scaling the free parameters r_s and ρ_s , which define a characteristic length and density, the NFW profile can describe dark matter haloes from dwarf galaxy to cluster scales. Furthermore, it was found the NFW profile was valid for haloes regardless not only of mass but also the power spectrum of initial density fluctuations and values of cosmological parameters, establishing that density profiles are universal in form independent of the cosmological context (Navarro et al. 1997). Another universal property was found in the coarse-grained phase-space density profile, $Q \equiv \rho/\sigma^3$, where σ is the velocity dispersion of simulation particles. Taylor & Navarro (2001) discovered Q has

a remarkably simple form of a power-law, $Q \propto r^\gamma$, with $\gamma \sim -1.9$.

It is useful to recast the free parameters of the NFW profile in terms of a halo mass and concentration. For relaxed haloes a radius can be defined in which the material has reached virial equilibrium:

$$M_{vir} = \frac{4\pi}{3} \Delta(z) \rho_c(z) R_{vir}^3, \quad (2)$$

where R_{vir} is the virial radius enclosing a density Δ times the critical density, ρ_c , at redshift z . The characteristic radius r_s can be recast as the concentration parameter, $c_{vir} \equiv R_{vir}/r_s$. Much effort has gone into understanding the relationship between c_{vir} and M_{vir} as well as the dependencies on the background cosmology and the evolution with redshift (Prada et al. 2012). This is necessary for predicting the properties of luminous galaxies that reside in the dark matter haloes and for using galaxy observations as probes of the cold dark matter (CDM) paradigm. The concentration was found to correlate with mass such that smaller mass haloes are more concentrated (Navarro et al. 1997). This was understood as a consequence of the earlier formation epoch of small mass haloes in the bottom-up structure formation of CDM. Since small haloes collapse ear-

* E-mail: Emil.Polisensky@nrl.navy.mil

† E-mail: ricotti@astro.umd.edu

lier, their inner regions reflect the higher universal density of matter at earlier times. Changing the cosmological parameters or the power spectrum changes the halo formation epoch and affects the concentrations but does not affect the shape of the universal profile (Polisensky & Ricotti 2014). This interpretation is consistent with simulations of hot and warm dark matter which found haloes with masses below the truncation scale form later and have lower concentrations than CDM haloes of similar size (Avila-Reese et al. 2001; Bode et al. 2001; Knebe et al. 2002).

Much effort has also gone into understanding the physical processes that produce the NFW profile. There are two main approaches to analytically modeling the density profile: smooth accretion based on spherical infall (Gunn & Gott 1972; Gott 1975), and hierarchical merging following Press-Schechter formalism (Press & Schechter 1974; Peebles 1974; Lacey & Cole 1993; Manrique et al. 2003). Both approaches have been successful at producing the universal profiles. This has been explained as a result of the process of virialization. If virialization erases all information about the past merging history of the halo then it does not matter if the mass accretion is modeled as clumpy or smooth. However, a consensus has not emerged on the dominant processes occurring during virialization or if the virialization process erases all memory of the initial conditions.

The early stages of halo formation are marked by rapid accretion and mergers making it natural to consider violent relaxation as the dominant mechanism determining the dark matter profiles in the fluctuating gravitational potential (White 1996). Violent relaxation was originally proposed to explain the structure of elliptical galaxies (Lynden-Bell 1967) where estimates of star-star encounters would not establish equilibrium in a Hubble time. The relaxation time of a forming halo is related to the rate of change of the gravitational potential. Austin et al. (2005) and Barnes et al. (2006) argue the universal nature of $Q(r)$ results from violent relaxation.

The works of Wechsler et al. (2002); Zhao et al. (2003, 2009) have shown there are two main eras of halo growth, a fast accretion phase and a slow phase. The fast growth phase in CDM is dominated by mergers of objects with similar mass in contrast to the slow growth phase characterized by quiescent accretion and minor mergers. The inner halo is set at the end of the fast era with the slow growth phase having little impact on the inner structure and gravitational potential well, leading to an inside-out growth of haloes. These studies find violent relaxation is only important in forming the inner profile with the outer profile determined by secondary infall during the slow growth phase.

The NFW profile is characterized by a logarithmic slope, $\alpha \equiv d \log \rho / d \log r$, that rolls from an asymptotic value $\alpha = -3$ at large radii to $\alpha = -1$ in the inner halo. The value of the inner slope has been a matter of controversy. The first concerned the value of the asymptotic slope (Moore et al. 1999). As the number of particles in simulations have increased it has become evident the density profiles do not approach an asymptotic value but continue to roll slowly with radius (Navarro et al. 2004; Diemand et al. 2004; Graham et al. 2006) and are better described by Einasto profiles (Einasto 1965). However, this has

not changed the conclusion that all information about the formation history is lost in the virialization process.

The second controversy is a dependence of the inner profile on the halo mass. Many models have been constructed that explain the emergence of the universal profile as a consequence of repeated mergers (Syer & White 1998; Nusser & Sheth 1999; Subramanian et al. 2000; Dekel et al. 2003). Although they differ in the details, the relevant physical processes determining the halo properties are the tidal stripping of material from accreting subhaloes, dynamical friction, and tidal compression transferring energy from the satellites to the halo particles and the decaying of satellite orbits to the halo centre. These models predict a dependence of the inner density profile slope on the slope of the power spectrum at the scale of the halo, $P(k) \propto k^n$. The steeper spectrum characteristic of dwarf-scales is predicted to produce softer cores than for galactic and cluster-scale haloes. Independent of the merger models, Del Popolo (2010) questions the universality of both the density and the Q profile and concludes both should depend on mass. His spherical infall models with angular momentum show a steepening of the inner density profile with increasing halo mass, although to a lesser extent than the merger models. The central question of these studies is, do haloes in equilibrium retain any memory of the initial conditions and mass function of accreting satellites they are built from or is all information lost in the virialization process?

Ricotti (2003) ran CDM simulations of the same realization of the density field in boxes of varying side length to compare the profiles at different mass scales. He examined the average profiles when the box structures showed similar clustering and the most massive haloes were composed of the same number of particles. He found a systematic dependence of the inner slope on halo mass with dwarf-scale haloes having softer cores than galactic and cluster-scale haloes in agreement with the predictions of Subramanian et al. (2000). These results were reinforced in Ricotti & Wilkinson (2004); Ricotti et al. (2007). Jing & Suto (2000) also saw a dependence of inner slope in their simulations of haloes at galactic and cluster scales.

Another way of testing the importance of substructure is by introducing a truncation in the power spectrum as in hot and warm dark matter (WDM) cosmologies where substructure is suppressed below the particle free-streaming scale and haloes form by monolithic collapse. Many investigations using these cosmologies have been conducted (e.g. Wang & White 2009, Huss et al. 1999b, Moore et al. 1999, Colín et al. 2000, Busha et al. 2007, Bode et al. 2001, Polisensky & Ricotti 2011). These works find haloes that form below the truncation mass have lower concentrations consistent with their later formation epochs but the profiles are well described by the NFW form. This is in contrast to Colín et al. (2008) who find the inner profiles are systematically steeper in their WDM simulations of Galaxy-sized haloes. Recent studies of CDM microhaloes confirm halo profiles near the streaming scale are steeper when a truncation is introduced into the power spectrum than without, however the origin of the steepening remains unclear (Ishiyama et al. 2010; Anderhalden & Diemand 2013; Ishiyama 2014). Independent models of the density profiles of WDM haloes predict not a steepening but a flattening of the inner profile due to the truncated power spectrum

(Williams et al. 2004; Viñas et al. 2012). It is important to stress the flattening in these models is due to the truncated power spectrum alone, not to the random thermal motions of WDM particles which were not included in the models.

In this work we employ N -body simulations of halo formation in CDM and WDM cosmologies to explore the effects of the power spectrum on halo structure and dynamics. We use the method of Ricotti (2003) of scaling the simulation volume to change the mass scale (§ 2). However, we do not study a statistical sample of haloes but focus on a handful of halos with about a factor of 100 greater mass resolution than in Ricotti (2003). The goal is not to rigorously test any particular halo model but simply to look for evidence the halo retains memory of the initial power spectrum. This evidence is expected to manifest itself as trends in the halo profiles as the mass and truncation scales change (§ 3). We examine if our results are typical of a larger halo population (§ 4) and investigate the physical origin of the results (§ 5). A discussion and comparison to previous published works is presented in § 6 and the summary in § 7.

2 NUMERICAL SIMULATIONS

2.1 Cosmological Models

WDM particles are relativistic in the early universe and free-stream out of overdense regions before the adiabatic expansion of the universe reduces the particles to subrelativistic velocities. WDM thus damps density perturbations below a characteristic scale that depends on the particle mass and acts as a filter on the power spectrum of density perturbations. The power spectra for WDM cosmologies is related to that for CDM by

$$P_W(k) = P_C T_W^2, \quad (3)$$

where T_W is the WDM transfer function. The transfer function given by Bode et al. (2001) is used for dark matter particles that were coupled to the relativistic cosmic plasma at early times and achieved thermal equilibrium prior to the time of their decoupling. The formula of Eisenstein & Hu (1998) is adopted for the CDM power spectrum.

We define the WDM filtering mass as in Sommer-Larsen & Dolgov (2001),

$$M_f \equiv \frac{4\pi^4}{3} \Omega_m \rho_c k_f^{-3}, \quad (4)$$

where ρ_c is the critical density and k_f is a characteristic free-streaming wave number defined where $T_W^2 = 0.5$. For consistency with Sommer-Larsen & Dolgov (2001) we also define the free-streaming, or filtering length as $R_f \equiv 0.46 k_f^{-1}$.

We adopted values for cosmological parameters from the Bolshoi simulation (Klypin et al. 2011), $(\Omega_m, \Omega_\Lambda, \Omega_b, h, \sigma_8, n_s) = (0.27, 0.73, 0.0469, 0.7, 0.82, 0.95)$, which were chosen to be within 1σ of WMAP5, WMAP7, and consistent with the results of supernovae, and X-ray cluster surveys. These parameters are also within 1.7σ of WMAP9 and 2.2σ of Planck1. We use a variety of WDM models for thermal relics in the range 0.75 – 66 keV.

Since our focus is to examine the effects of the power spectrum on halo structure, the initial conditions include particle velocities due to the gravitational potential using the Zeldovich approximation but random thermal velocities

appropriate for WDM have not been added to the simulation particles. For the WDM cosmologies adopted here the effects of thermal velocities are expected to be small; this is discussed further in Section 6.

2.2 Software

The simulations were conducted with the N -body cosmological simulation code GADGET-2 (Springel 2005) with gravitational physics only and initial conditions generated with the GRAFIC2 software package (Bertschinger 2001). We produce a single realization of the density field but vary the power spectrum of fluctuations appropriate for CDM and WDM cosmologies.

The AMIGA’s Halo Finder (AHF) software (Knollmann & Knebe 2009) was used to identify and characterize all gravitationally bound haloes composed of at least 50 particles after iteratively removing unbound particles. The virial mass of a halo is defined in Equation 2. Since the simulations are confined to high redshifts ($z > 3$) the universe is matter dominated at all epochs and we adopt the virial condition for an Einstein-de Sitter cosmology, $\Delta(z) = 178$. The MergerTree tool in AHF was used to construct merger trees, identify halo progenitors at all times, and for identifying haloes across cosmologies.

AHF calculates the convergence radius according to the criterion of Power et al. (2003) and is generally about 10 softening lengths, enclosing ~ 2000 particles at $r \sim 0.006 R_{vir}$. We tested this by running low resolution simulations and found that the profiles are actually converged to about 5–6 softening lengths, enclosing ~ 200 particles at $r \sim 0.003 R_{vir}$. The convergence radius given by AHF may be overly conservative for the simulations but this has no impact on the results. When examining the halo profiles we adopt the convention of plotting $r > 6\epsilon$ but indicating in bold where the profiles satisfy the criterion of Power et al.

2.3 Simulations

We simulated a small cubic box with a comoving side length of 3.3 Mpc from $z = 79$ to $z = 8$ with 512^3 particles and mass resolution $\sim 10^4 M_\odot$. A halo of mass $\sim 2 \times 10^8 M_\odot$ that appeared to have an early formation epoch and relaxed to virial equilibrium at scale factor $a = 0.1$ ($z \equiv a^{-1} - 1$) was chosen for resimulation using a zoom technique. We refer to this as “Halo A.” A volume of higher mass resolution was generated in the initial conditions covering the initial volume of particles that end within three virial radii of Halo A. We ran high resolution simulations with a mass resolution of $18.7 M_\odot$ in CDM and multiple WDM cosmologies in the range 4–66 keV. We adopted a force softening length of 8 pc, held constant in comoving units. To test the convergence of our results we also ran low resolution simulations with the mass resolution reduced by a factor of 8 in CDM and 6 keV WDM. We further tested the dependence of our results on the initial conditions by running low resolution tests in CDM and 6 keV starting from $z = 120$.

We ran additional simulations with the box size increased to medium and large side lengths of 7.0 and 22.4 Mpc to increase the mass scale a factor of 10 and 320, respectively. The force softening lengths were also scaled with the box size

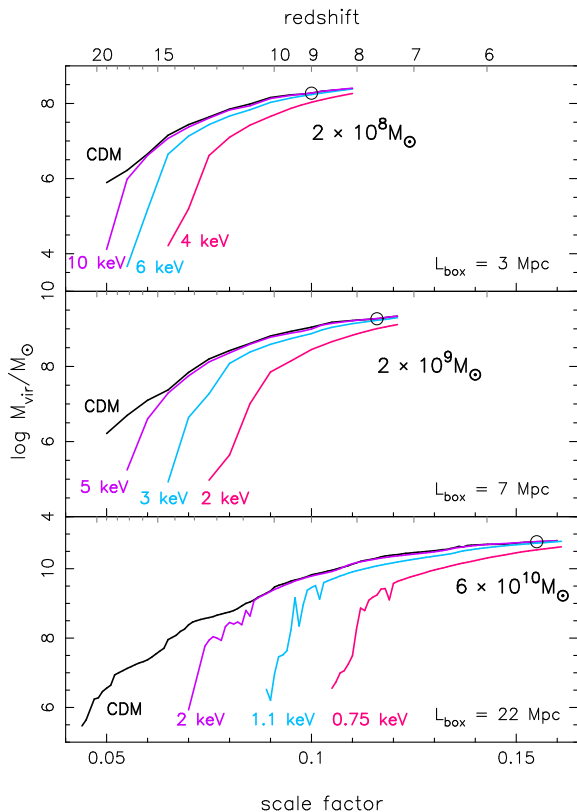


Figure 1. Mass growth of Halo A in the small, medium, and large box simulations (top to bottom) in CDM and select WDM cosmologies. The circles show the CDM halo at the normalization times when the halo has grown to $\sim 10^7$ particles at the three mass scales.

to 17 pc and 55 pc, respectively. CDM and WDM cosmologies ranging from 2 – 5 keV were run for the medium mass scale while CDM and 0.75 – 2 keV WDM were run for the large mass scale. To compare Halo A across mass scales we define “normalization times” as the epochs when the CDM haloes have grown to encompass the same number of particles within the virial radius, $N \sim 10^7$, as the small mass scale at $a = 0.1$. This occurred at $a = 0.116$ and $a = 0.155$ for the medium and large scales, respectively. Figure 1 shows the growth of Halo A for the three mass scales. Halo formation is delayed in the WDM cosmologies. However, once it begins it grows quickly until it catches up with the CDM halo, after which it evolves at a similar rate. The circles show the normalization times when the halo has entered the slow-growth phase and has reached the same size in CDM at all scales. At the normalization times the halo masses are approximately $2 \times 10^8 M_\odot$, $2 \times 10^9 M_\odot$, and $6 \times 10^{10} M_\odot$ for the small, medium, and large mass scales, respectively.

Table 1 gives a summary of the simulations conducted in this work. Listed in the table are the WDM filtering mass, the filtering length, and the number of simulation particles sampling the filtering mass, N_f . For the WDM cosmologies the box side length L_{box} is given in units of the filtering length. This is a convenient way to show in which simulations the effects of the truncated power spectrum will be similar across mass scales. The 2 keV simulation in the large box is expected to be similar to the 5 keV medium box and 10 keV small box. Likewise, the 1.1 keV large box will be

Table 1. Properties of simulations.

Cosmo	M_f [M_\odot]	R_f [kpc]	N_f [$\times 10^7$]	L_{box}
(1)	(2)	(3)	(4)	(5)
<i>Small Box: $m_{res} = 18.7 M_\odot$</i>				
CDM	-	-	-	3270 kpc
66 keV	1.90×10^4	0.7	10^{-4}	$4485 R_f$
34 keV	1.90×10^5	1.6	0.001	$2082 R_f$
21 keV	9.50×10^5	2.7	0.005	$1217 R_f$
15 keV	3.19×10^6	4.0	0.02	$812 R_f$
10 keV	1.29×10^7	6.4	0.07	$510 R_f$
7 keV	4.43×10^7	9.7	0.2	$338 R_f$
6 keV	7.54×10^7	11.5	0.4	$283 R_f$
5 keV	1.41×10^8	14.2	0.8	$230 R_f$
4.5 keV	2.03×10^8	16.1	1.1	$203 R_f$
4 keV	3.05×10^8	18.4	1.6	$178 R_f$
<i>Medium Box: $m_{res} = 187 M_\odot$</i>				
CDM	-	-	-	7049 kpc
5 keV	1.41×10^8	14.2	0.08	$495 R_f$
3 keV	8.24×10^8	25.6	0.4	$275 R_f$
2 keV	3.34×10^9	40.8	1.8	$173 R_f$
<i>Large Box: $m_{res} = 6,010 M_\odot$</i>				
CDM	-	-	-	22394 kpc
2 keV	3.34×10^9	40.8	0.06	$548 R_f$
1.1 keV	2.63×10^{10}	81.2	0.4	$276 R_f$
0.75 keV	9.84×10^{10}	126.2	1.6	$177 R_f$

similar to the 3 keV medium box and 6 keV small box. The 0.75 keV large box will be similar to the 2 keV medium box and 4 keV small box. These simulations are colour-coded in Figure 1 according to their ratios of box scale to WDM filtering scale. Another way of characterizing the similarity of these simulations is by the ratio of filtering mass to halo virial mass. This ratio is equivalent to N_f expressed in units of 10^7 , as listed in column (4) of Table 1. For the similar cosmologies given above, the filtering masses are approximately 7%, 40%, and 170% of the halo masses at the normalization times.

Table 2 summarizes the properties of Halo A at the normalization times. An examination of Figure 1 shows Halo A has not suffered a recent major merger and is in the slow growth phase in all cosmologies at the normalization times. However, a more rigorous examination of the halo relaxation state is desirable. Differences from a universal profile are seen in unrelaxed haloes and haloes with large amounts of substructure (Jing 2000). Additionally, the inner slope of the density profile is sensitive to the location of the halo centre. An artificial flattening of the profile could be produced by an ambiguously defined centre due to a recently arrived subhalo at the core, for example. We performed a qualitative visual examination that the halo centres determined by AHF correspond to the density peak of particles and we examined quantitative measures of the relaxation. Studies with large samples of haloes have identified several metrics for separating haloes by relaxation state (Neto et al. 2007; Macciò et al. 2007, 2008): x_{off} , the offset between the halo centre and centre of mass of particles within R_{vir} ; the

Table 2. Properties of Halo A at the normalization times in the high resolution simulations.

Cosmo	M_{vir} [$10^8 M_\odot$]	λ' [10^{-2}]	x_{off} [R_{vir}]	$\frac{2K}{ U } - 1$	f_{sub}
(1)	(2)	(3)	(4)	(5)	(6)
<i>Halo A - Small Box</i>					
CDM	1.868	4.21	0.06	0.41	0.08
66 keV	1.847	3.84	0.05	0.40	0.07
34 keV	1.863	3.89	0.05	0.40	0.06
21 keV	1.882	3.99	0.06	0.39	0.05
15 keV	1.888	4.24	0.05	0.42	0.05
10 keV	1.887	4.63	0.08	0.42	0.05
7 keV	1.811	4.88	0.08	0.40	0.04
6 keV	1.713	4.80	0.07	0.40	0.03
5 keV	1.507	4.30	0.06	0.39	0.03
4.5 keV	1.330	3.93	0.06	0.39	0.03
4 keV	1.074	3.16	0.06	0.41	0.05
<i>Halo A - Medium Box</i>					
CDM	18.533	4.09	0.06	0.39	0.08
5 keV	18.894	4.63	0.06	0.41	0.05
3 keV	16.912	4.76	0.07	0.40	0.04
2 keV	10.126	3.10	0.05	0.40	0.05
<i>Halo A - Large Box</i>					
CDM	600.497	3.34	0.04	0.39	0.13
2 keV	604.681	4.07	0.08	0.40	0.05
1 keV	547.367	4.44	0.07	0.39	0.03
0.75 keV	351.273	3.48	0.04	0.38	0.05

virial ratio $2K/|U| - 1$; the mass fraction bound in subhaloes f_{sub} ; and the spin parameter, λ' , that characterizes the halo angular momentum (Bullock et al. 2001):

$$\lambda' = \frac{J}{\sqrt{2}M_{vir}v_{vir}R_{vir}}, \quad (5)$$

where J is the total angular momentum of all particles within R_{vir} and v_{vir} is the circular velocity at R_{vir} , $v^2 \equiv GM/R$. These metrics are listed in Table 2. The general conditions for a relaxed halo are: $\lambda' < 0.1$, $x_{off} < 0.07R_{vir}$, $2K/|U| - 1 < 0.35$, and $f_{sub} < 0.1$ (Ludlow et al. 2012, 2013, 2014). Halo A largely satisfies these criteria with the greatest discrepancy being a slightly larger virial ratio of ~ 0.4 , however in Section 4 we examine the stability of the profiles and find our results are not due to the relaxation state of the halo or transient accretion events.

We note a curious increase in f_{sub} for the warmest cosmologies in all three box sizes. We examined this further by applying varying subhalo mass cuts and found f_{sub} is dominated by subhaloes with less than 5000 particles in these cosmologies. Artificial haloes of this size are known to form along filaments in truncated power spectrum cosmologies (Wang & White 2007) and are likely contaminating f_{sub} .

3 RESULTS I - NON-UNIVERSALITY OF PROFILES

We begin by examining the effects of the WDM power spectra on the density structure of Halo A in the three boxes and thus the three mass scales of the halo. We then examine the kinematics and conclude by checking the convergence. In Section 4 we examine a larger halo sample to check if the results of Halo A are typical for haloes in general and we show the features in the profiles are dynamically stable.

3.1 Density Structure

The left panel of Figure 2 shows the spherically averaged density profiles of Halo A at $a = 0.1$ in all cosmologies for the small mass simulations, $M = 2 \times 10^8 M_\odot$. The profiles are plotted with solid lines where they satisfy the convergence criterion of Power et al. (2003) and the inner profiles are extended to six force softening lengths with dotted lines. Excellent agreement is seen between the high and low resolution CDM profiles. No significant differences from CDM are seen for a filtering mass 10^{-4} of the halo mass. As the filtering mass increases the inner profile at $r < 0.1R_{vir}$ steepens and the density increases. The location where the WDM density begins to increase shows a correlation with filtering scale, moving to larger radii as the cosmology gets warmer and the filtering scale larger. In the range $0.1 - 0.4R_{vir}$ the WDM densities fall below that of CDM while the densities agree with CDM for $r > 0.4R_{vir}$ except in the warmest cosmologies where the halo outskirts are still growing by secondary infall. These features are more pronounced in the cumulative mass profiles shown in the right panel of Figure 2. The enclosed mass is equivalent in CDM and WDM at $> 0.5R_{vir}$ indicating it is the mass in shells at $0.1 - 0.4R_{vir}$ that has been displaced to smaller radii in the WDM simulations.

To compare the mass profiles of Halo A across the three mass scales we plot in the left panel of Figure 3 the profiles of enclosed number of simulation particles and normalize the radial coordinates by the CDM virial radius in each box. Interestingly, variations are seen at $r < 0.1R_{vir}$ in the CDM haloes as a function of the halo mass in contrast to the WDM simulations where the profiles are nearly identical across the explored halo mass range. The enclosed mass in the CDM inner halo becomes greater as the halo mass increases but when small scale structures are erased, as in the WDM simulations, the mass profiles are insensitive to the halo mass. Angular momentum sets the shape of the inner profile in the models of Del Popolo (2009) where more massive haloes are predicted to have less angular momentum resulting in steeper profiles. It can be seen from Table 2 that the spin of the CDM halo decreases as the mass scale increases, consistent with this idea.

The CDM halo spin parameter is 26% higher at the small mass scale compared to the large while the WDM haloes vary by $\lesssim 10\%$ which may be why the WDM profiles are very similar. However, the WDM spin parameters are generally higher than the CDM halo at all scales yet they have steeper profiles than CDM so this is not the entire answer. One difficulty is the spin parameter includes all particles within the virial radius while the greatest differences between profiles are seen in the inner halo. This is examined further in Section 5.

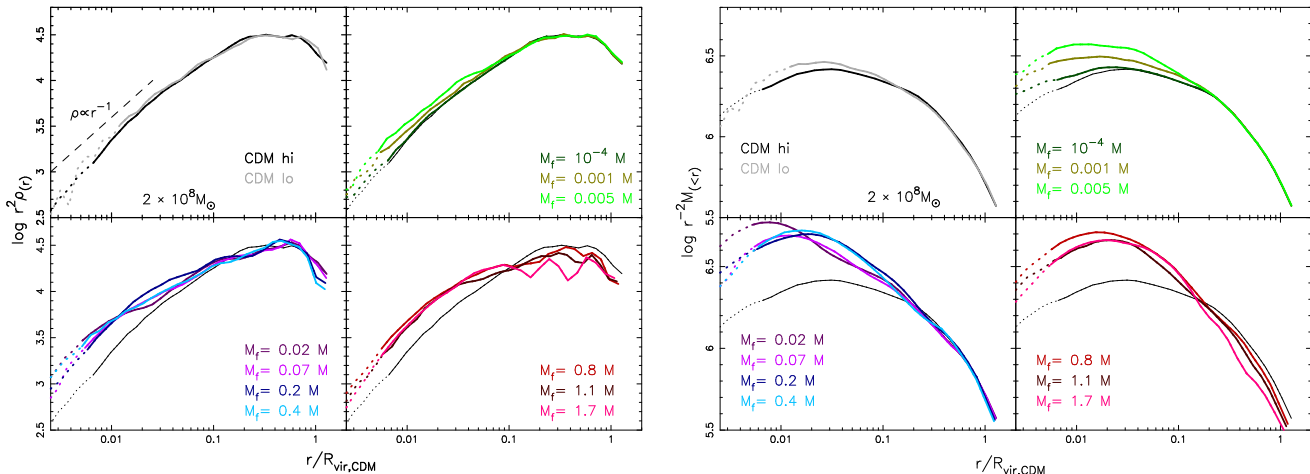


Figure 2. (Left) Density profiles of the small mass simulations of Halo A at the normalization time, $a = 0.1$. The dashed line gives the asymptotic slope of the NFW profile at small radii. (Right) Cumulative mass profiles of the small mass simulations of Halo A. The density profiles have been multiplied by r^2 and the mass profiles by r^{-2} to reduce the dynamic range. The radial coordinates have been normalized to the virial radius in CDM and are plotted to six softening lengths (6ϵ). The WDM profiles have been grouped and are plotted against the CDM profile for clarity. All profiles are plotted with solid lines where they satisfy the convergence criterion of Power et al. (2003). As the filtering mass increases clear deviations from a universal shape are seen in the WDM profiles caused by the displacement of mass from intermediate radii to the core in the WDM simulations.

It is important to emphasize that the differences between WDM and CDM profiles diminish as the halo mass increases due to the steepening of the CDM profile. This observation may explain why previous works have not clearly identified the prominent features and trends in the profile shapes found in this work and the recent simulations of microhaloes near the CDM filtering scale (Ishiyama et al. 2010; Anderhalden & Diemand 2013; Ishiyama 2014).

In the right panel of Figure 3 the logarithmic slope of the density profiles are compared across mass scales for a given ratio M_f/M . The large mass CDM halo profile is steeper than the medium and small haloes for $r < 0.3R_{vir}$ and reaches the NFW value of -1 at a smaller radius (given by the vertical short grey lines). However, the differences are less than predicted by the model of undigested subhalo cores of Subramanian et al. (2000) but in agreement with the predictions of the angular momentum models of Del Popolo (2010).

Unlike the CDM profiles the slopes in the WDM cosmologies are nearly identical across mass scales. For $M_f < M$ the slopes tend toward plateaus of constant value when moving to smaller radii. These plateaus also depend on the filtering scale, ranging from $r = 0.02 - 0.1R_{vir}$ for $M_f \sim 0.07M$ but grow steeper and move outward to $r = 0.04 - 0.3R_{vir}$ for $M_f \sim 0.4M$. These tendencies were also seen in the CDM microhalo simulations of Ishiyama (2014). They fit a power law function to the relation between halo mass and inner slope α for their sample:

$$\alpha = 0.123 \log(M_{vir}/M_f) - 1.461, \quad (6)$$

with a scatter of 20%. We plot the values given by this equation as horizontal arrows in the right panel of Figure 3 and find agreement with the slope plateaus to 10%.

Our simulations also show interesting new features in regimes not explored in Ishiyama (2014). Continuing to smaller radii the slopes do not remain at the asymptotic values of the plateaus but soften. The slopes remain steeper

than CDM for $r < 0.1R_{vir}$ and achieve -1 at smaller radii, although this scale moves outward as the filtering scale gets larger. The inner profiles quickly become softer than CDM at $r \lesssim 0.01R_{vir}$. The inner profiles are shallower in WDM in agreement with the models of Williams et al. (2004) and Viñas et al. (2012). For $M_f > M$ the slope profiles do not form a plateau but remain steeper than CDM for $r > 0.01R_{vir}$.

3.2 Internal Kinematics

Figure 4 shows the profiles of σ^3 for the small mass simulations of Halo A, where σ is the local 3D velocity dispersion. Similar to the density profiles, the dispersions are greater in the inner WDM haloes compared to CDM and show a correlation with the filtering scale, growing larger and extending to greater radii as the cosmology becomes warmer and the filtering scale increases. This can be understood as a consequence of the increased mass in the WDM cores. As the mass in the core grows the dispersion must get larger to stay in virial equilibrium against the deeper potential well.

To examine the phase space density profiles of Halo A we adopt $\gamma = -1.875$ and fit the profiles of each CDM halo to the form, $Q_{fit} = Ar^\gamma$. For illustrative purposes we show Q normalized to the power law fit, $\tilde{Q} = Q/Q_{fit}$, to emphasize deviations from a simple power law. We calculate \tilde{Q} for the WDM simulations using the CDM Q_{fit} . The left panel of Figure 5 shows the deviations from power law for Halo A in common cosmologies for all three mass scales. A prominent feature is seen in the inner regions of the WDM haloes, reaching a maximum deviation before declining. Along the top axis of each plot are ticks marking the location of $0.037R_f$ in each WDM cosmology. This scaling was empirically determined but marks the location of the peak remarkably well indicating the deviations scale with the filtering scale.

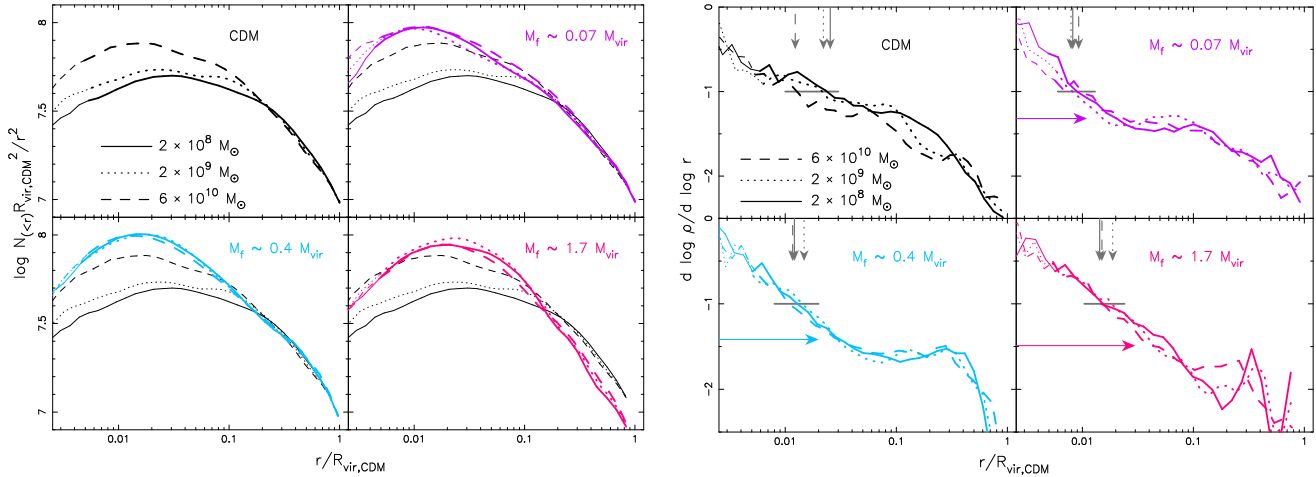


Figure 3. (Left) Comparison of the cumulative mass profiles of Halo A at the normalization times of the three mass scales when the haloes have grown to $\sim 10^7$ particles. The small, medium, and large mass haloes are plotted with the solid, dotted, and dashed lines, respectively. The profiles are given by the number of enclosed simulation particles and the radial coordinates have been normalized by the CDM virial radii. The WDM profiles are plotted against the CDM profiles for comparison. (Right) Comparison of the slope of the density profiles of Halo A across the three mass scales at the normalization times. Short grey lines and vertical arrows indicate where the log slope is -1 in all cosmologies. The CDM halo is steeper at the large mass scale than the small scale. The WDM haloes are generally steeper than the CDM but soften at $r < 0.01 R_{vir}$. Horizontal arrows show the fitting formula of Ishiyama (2014) and match the WDM plateaus to 10%.

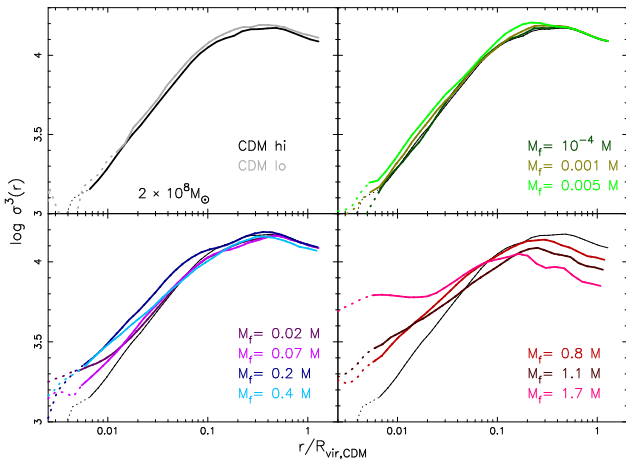


Figure 4. Velocity dispersion profiles of the small mass simulations of Halo A. WDM simulations have been grouped and plotted against the CDM profile for clarity.

Interestingly, a drop in the inner profile of the CDM haloes is seen that becomes more pronounced as the halo mass decreases. This also agrees with the models of Del Popolo (2010) that demonstrate a dependence of the Q profile on halo mass.

A useful metric of the particle orbits is the velocity anisotropy parameter given by:

$$\beta(r) = 1 - \frac{\sigma_\theta^2 + \sigma_\phi^2}{2\sigma_r^2}, \quad (7)$$

where σ_θ^2 and σ_ϕ^2 are the angular velocity dispersions and σ_r^2 is the radial velocity dispersion. For purely radial orbits, $\beta = 1$, while isotropic particle motions give $\beta = 0$. At the halo outskirts $\beta \rightarrow 1$ where freshly accreted material is still falling inward while in the core of a relaxed halo $\beta \rightarrow 0$.

In practice the anisotropy parameter is seldom exactly zero in the inner regions since simulated haloes are generally not spherically symmetric.

The right panel of Figure 5 shows the velocity anisotropy profiles of Halo A at common filtering scales in all simulations. There is a radial bias in the CDM particle orbits at $r > 0.1 R_{vir}$ while particles inside this scale are well isotropized. The WDM anisotropy profiles are generally similar to CDM, although in the warmest cosmologies (bottom row) the haloes have radial bias extending deeper into the inner halo than in the other cosmologies. An examination of the halo shapes revealed a tendency for the haloes to become more spherical in the inner and outer regions at $r < 0.02 R_{vir}$ and $r > 0.2 R_{vir}$ and less spherical in the intermediate regions as the filtering mass increases. The features of the velocity anisotropy may thus not be due to an incomplete isotropization of the particle velocities but simply to the increased triaxiality seen at these radii. What is clear is the lack of any feature at the location of the peak deviations in the Q profile making it apparent the physical processes that created the increased mass in the WDM cores do not leave an imprint on the isotropy of particle velocities after virialization.

3.3 Convergence Tests

Figure 6 shows the profiles of Halo A in the high and low resolution simulations and the test simulations initiated from a higher redshift. Excellent agreement is seen across resolutions in both CDM and WDM and from the simulations started from higher redshift. The convergence criterion of Power et al. (2003) tested on CDM simulations appears to be not only valid but perhaps overly conservative in measuring the convergence radii of our WDM simulations.

Simulations with truncated power spectra are known to

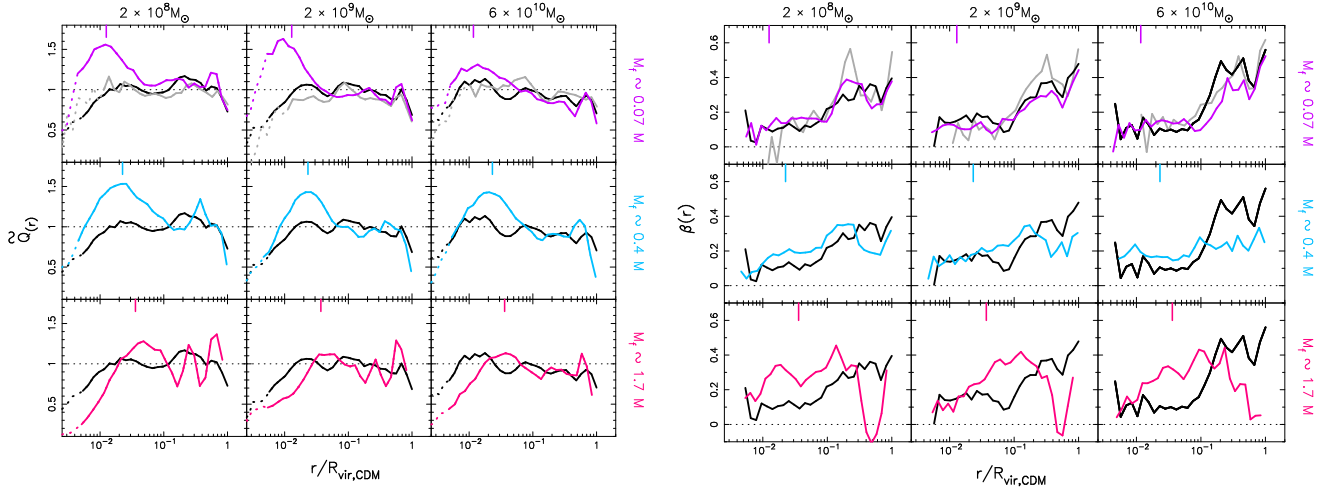


Figure 5. (Left) Deviations from power-law behaviour in the phase space density profiles of the simulations of Halo A. (Right) Velocity anisotropy profiles of the simulations of Halo A. The simulations are grouped by mass scale: small, medium, and large from left to right, and by relation of filtering mass to halo mass with the cosmology growing warmer from top to bottom. Deviations from power-law are seen in the inner WDM haloes that reach a peak at $\sim 4\%$ of the filtering length (coloured ticks along the top of each plot). However, no corresponding features are seen in the velocity anisotropy.

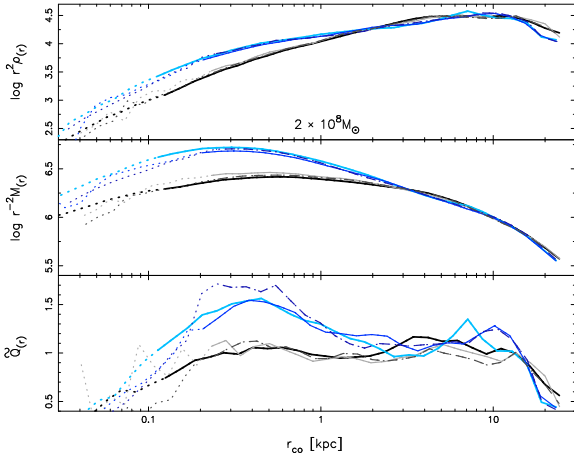


Figure 6. Comparison of the high and low resolution small mass simulations of Halo A. The high and low resolution CDM simulations are plotted in black and grey, respectively, the high and low 6 keV simulations in light and dark blue. The dashed lines are the low resolution 6 keV and CDM simulations started from a higher redshift. Profiles are plotted with solid lines where they satisfy the convergence criterion of Power et al. (2003) and are extended to 3σ with dotted lines. Consistent results are seen across simulations demonstrating the results are not affected by the mass resolution or starting redshift.

produce numerically artificial small mass haloes along the filaments of collapsed density perturbations (Wang & White 2007) whose size and separation are dependent on the mass resolution. Figure 6 also shows the results are not due to these spurious haloes since a dependence on the mass resolution would be expected to reflect on the shape and location of the features in the WDM profiles.

4 RESULTS II - TESTING COSMIC VARIANCE

To explore if the results for Halo A were typical of haloes in general we simulated two additional haloes, Halo B and Halo C. We first ran a low resolution simulation with a cubic refinement volume of side length $1/4$ the box length, composed of 512^3 particles, and centred on Halo A. The 15 largest haloes in the refinement volume were examined in detail. Two haloes were chosen based on their quiescent accretion histories and relaxation metrics for individual resimulation at high resolution in an analogous way to Halo A but only at large mass scale and only in CDM, 1.1 keV and 0.75 keV cosmologies. Haloes B and C grow to about the same size as Halo A by the end of the simulations but have later formation epochs suggesting Halo A forms from a volume with greater initial overdensity. For example, the 0.75 keV large scale Halo A grows to $N = 10^6$ at $a = 0.125$ while Haloes B and C don't reach this size until $a = 0.148$ and 0.165 , respectively.

We ran the large scale simulations of Haloes B and C to $a = 0.25$ to test the stability of the profiles over a greater time span than the simulations on Halo A presented in Section 3. To test the dynamical stability of Halo A we ran an extended simulation set at small mass scale for CDM, 6 keV and 4 keV WDM. The refinement volume was increased a factor of two to allow Halo A to evolve to $a = 0.125$ while preventing contamination by accretion of particles from outside the refinement volume. Snapshots of the particle data were saved every 0.001 change in scale factor. We list the properties of all three haloes at the end of their simulations in Table 3.

Figure 7 shows the density profiles and slopes for Haloes B and C and give excellent agreement with the results from Halo A. The slopes of the WDM profiles show the same tendency to steepen, reach a plateau, then soften in the inner halo, and show the same dependence on filtering scale. The density profiles similarly show the same characteristic fea-

Table 3. Properties of the small scale Halo A and large scale Haloes B and C at the end of each extended simulation set.

Cosmo	M_{vir} [$10^8 M_\odot$]	λ [10^{-2}]	x_{off} [R_{vir}]	$\frac{2K}{ U } - 1$	f_{sub}
(1)	(2)	(3)	(4)	(5)	(6)
<i>Halo A – Small Box – $a = 0.125$</i>					
A CDM	3.789	4.87	0.07	0.41	0.04
A 6 keV	4.029	4.86	0.04	0.40	0.01
A 4 keV	3.362	3.25	0.04	0.37	0.01
<i>Haloes B & C – Large Box – $a = 0.25$</i>					
B CDM	802.734	1.96	0.03	0.24	0.09
B 1.1 keV	708.649	1.77	0.02	0.21	0.01
B 0.75 keV	565.010	1.23	0.04	0.21	0.01
C CDM	572.440	2.72	0.05	0.21	0.12
C 1.1 keV	451.046	2.78	0.06	0.19	0.02
C 0.75 keV	308.477	1.45	0.02	0.17	0.01

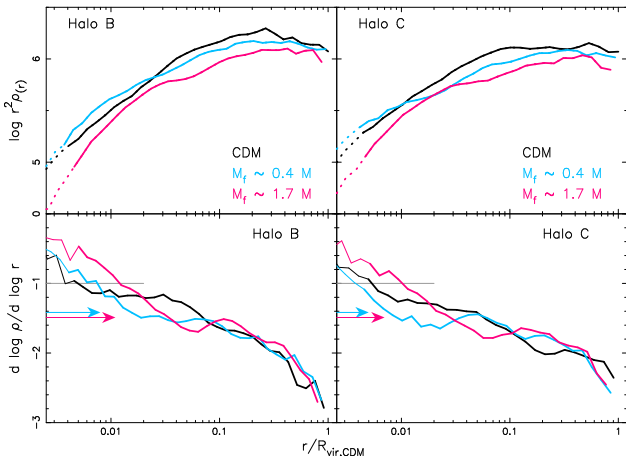


Figure 7. (Top) Density profiles of Haloes B and C in the large box-size simulations. The density profiles have been multiplied by r^{-2} to reduce the dynamic range. (Bottom) Slope of the density profiles for the same two halos.

ture of mass displaced from intermediate regions to the core in the WDM cosmologies. The main difference is a stronger deviation from CDM with a larger overall reduction in densities. The density profiles are everywhere below the corresponding CDM halo for the 0.75 keV cosmologies. Halo C shows a larger deviation from CDM than Halo B, likely related to the later formation epochs of these haloes.

We show the normalized phase space density profiles, \tilde{Q} , in Figure 8 for all three haloes in their CDM and WDM simulations at times when the haloes are composed of $> 10^5$ particles. The values of γ for Q_{fit} were determined separately for each halo by fitting the CDM profiles at late times. The CDM profiles of all three haloes are consistent with minor fluctuations about power laws while the large deviation seen in the WDM core of Halo A and its dependence on the filtering scale is also seen in the other two haloes.

The prominent feature of the 6 keV WDM core first appears in the profile of small scale Halo A at $a = 0.075$,

and at $a = 0.115$ in the large scale 1.1 keV Haloes B and C. After its formation the core feature is stable through the end of the simulation, spanning a time range of 420 Myr for Halo A and 1520 Myr for B and C. The dynamical time, $t_{dyn} = \sqrt{R^3/GM}$, for the core of Halo A is 6.5 Myr and 14-18 Myr for the cores of Haloes B and C, demonstrating the profiles are stable over at least 65 – 85 dynamical times. In the warmer cosmologies the cores form later but are also stable through the end of the simulations.

The mass growth rates, $\dot{M} \equiv d \log M / d \log a$, when the core features appear in the WDM profiles are $\dot{M} = 6 - 10$. At earlier times the growth rates are higher and the profiles fluctuate wildly. The fast and slow growth phases of Zhao et al. (2003) correspond to growth rates in the matter dominated era of $\dot{M} = 6$ and $\dot{M} = 1.5$, respectively. Our result that the core features appear as the growth rate slows supports this inside-out view of halo growth.

We conclude the structural and dynamical features of Halo A are valid for haloes near the filtering scale of WDM cosmologies in general and form as haloes transition from fast growth to the slow accretion phase, remaining stable thereafter.

5 ORIGIN OF THE CORE

The simulations in this work have shown changes in the density and dynamical profiles in the core is common for haloes near the filtering mass in WDM cosmologies. The previous section determined the formation time of the core and demonstrated its stability with time. In this section we investigate clues to the core’s origin.

We examine the cores of Halo A in the extended small scale simulations and the cores of Halo B and C at large mass scale. We define the proper radius of the core as 60 pc for Halo A, 680 pc for Halo B, and 400 pc for Halo C. These radii were held constant in proper length and the number of particles within each core was calculated for all cosmologies at all times a halo progenitor was identified. The top row of Figure 9 shows the growth in core particles in the CDM and WDM simulations. It is clear the core forms quickly in WDM while the core is built-up more gradually in CDM. The number of core particles remain approximately constant after formation in both CDM and WDM. The epoch of WDM core formation occurs shortly after the halo virial mass catches up to the CDM halo and the growth rate slows to the CDM rate. For example, in the 6 keV small mass scale simulation of Halo A the core forms at $a \sim 0.075$, while Figure 1 shows the growth rate slows to approximately the CDM rate at about the same time. This agrees with the formation epoch of the core feature in the \tilde{Q} profiles.

We characterize the angular momentum of each core with the dimensionless spin parameter, Eqn. 5, and compare the evolution of each core spin in the bottom row of Figure 9. There is a clear trend between the number of core particles and core spin. All cores tend to lose angular momentum over time but cores with fewer particles consistently have higher spin. There is also a trend that as the filtering scale increases the number of core particles first increases then decreases. This is most evident in Haloes B and C and is again likely due to the later collapse epochs of these haloes.

In Figure 10 we show the core particles of Halo A in the

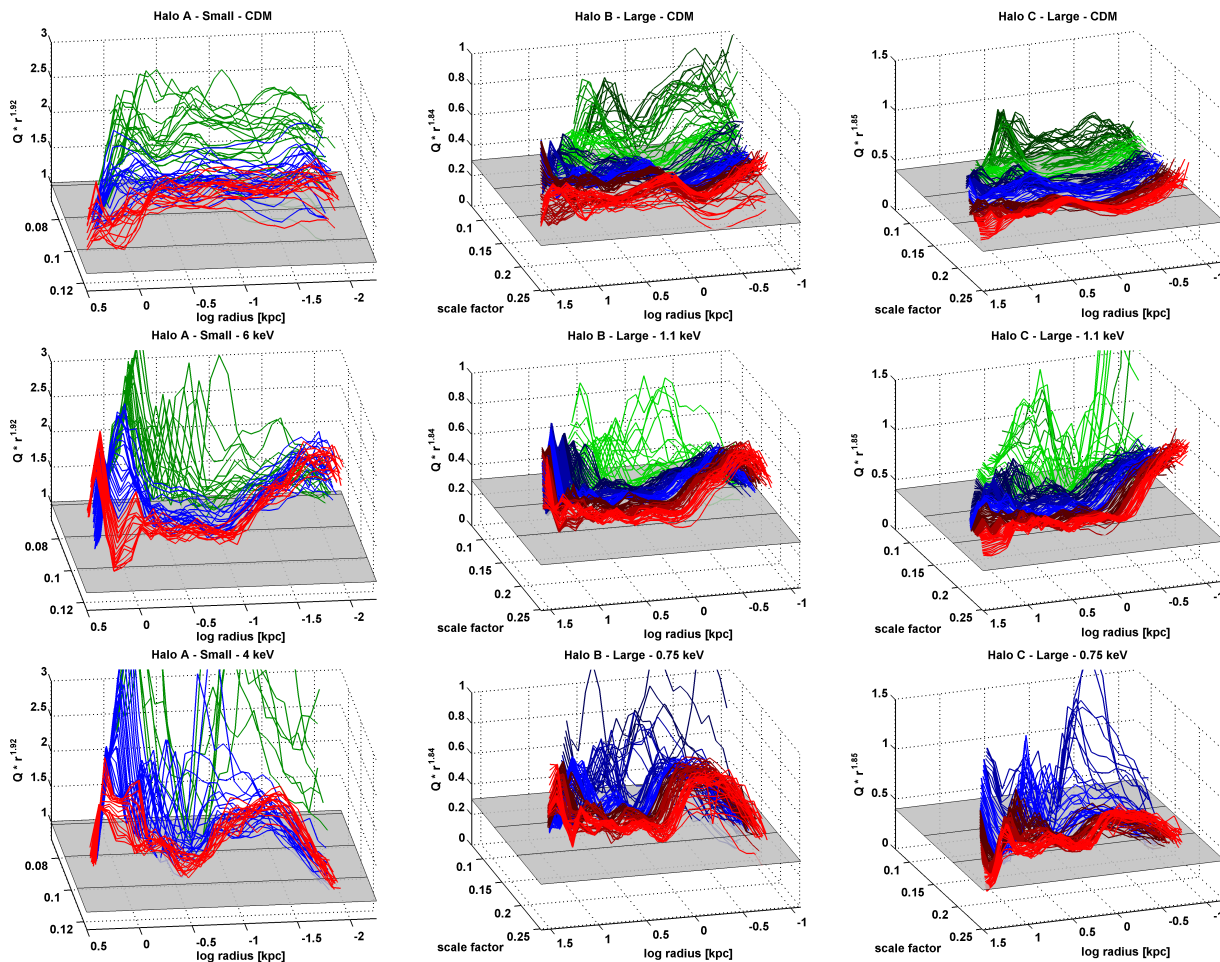


Figure 8. Evolution of the phase space density profiles of Halo A at small scale and Haloes B and C at large scale (left to right). CDM cosmologies are plotted in the top row, WDM in the bottom rows with filtering scale increasing top to bottom. The phase space density profiles have been multiplied by r^7 to show deviations from power law behaviour. The CDM profiles are consistent with power laws with minor fluctuations while the WDM profiles show prominent features in their cores that form shortly after the growth rate slows and are stable thereafter. Profiles are plotted with variable colour simply for visual clarity.

small mass scale simulations at $a = 0.05$, well before core formation. The images are centred on the particles' centre of mass. As noted by Busha et al. (2007), the filtered power spectra cause what were multiple clumps in CDM to become one collapsing clump in WDM. The core particles additionally become more symmetrically distributed around the centre of mass as the cosmology becomes warmer.

This evidence argues for angular momentum playing an important role in determining the structure of the core. The importance of angular momentum for the shape of the inner profile has been emphasized by a number of studies (Huss et al. 1999b,a; Hiotelis 2002; Ascasibar et al. 2004; Lu et al. 2006). Purely radial orbits give a steep inner profile, $\rho \propto r^{-2.25}$ (Bertschinger 1985). As the amount of angular momentum is increased particles remain closer to their maximum orbital radii resulting in shallower density profiles. Angular momentum is dominated by the tangential component of the velocity dispersions which are acquired dynamically in both the CDM and WDM simulations since thermal velocities were not added to the WDM particles. Interactions with substructure and the global tidal field produce tangential components to the particle velocities. An alter-

native possibility is radial orbit instability (Belokurov et al. 2008). A detailed study of particle orbits is outside the scope of this paper, however, after particles collapse the virialization process isotropizes their velocities equally well in both CDM and WDM as seen from Figure 5. The higher accretion rates in the WDM fast growth phase may also play a role in generating the core as seen in the models of Lu et al. (2006).

6 DISCUSSION

We found the inner structures of dark matter haloes in cosmologies with truncated power spectra deviate from their profiles in non-truncated cosmologies with mass displaced from the intermediate regions to the centre. We have already shown how our results are in agreement with previous work on CDM microhaloes (Ishiyama et al. 2010; Anderhalden & Diemand 2013; Ishiyama 2014), in this section we discuss how our work compares to other WDM and HDM studies.

Investigations of Milky Way satellites in 1–4 keV WDM

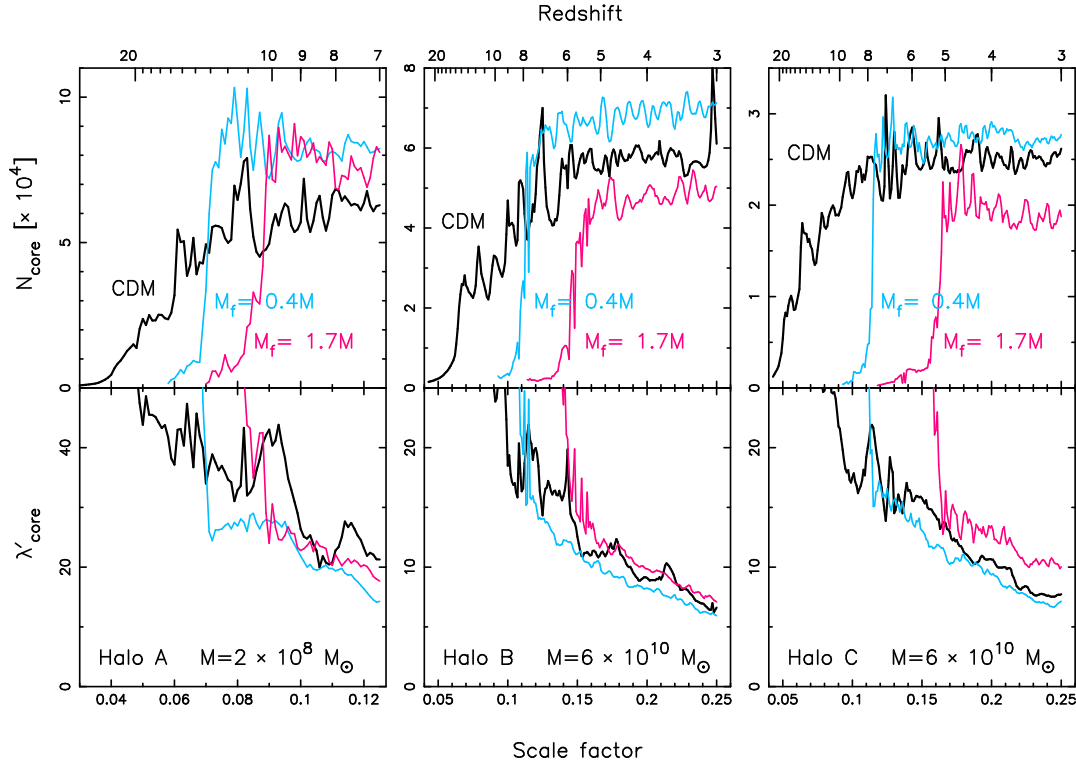


Figure 9. Evolution of the number of particles within the core (top) and the spin parameter of the core (bottom) in the extended small mass scale simulations of Halo A and large mass scale simulations of Haloes B and C (left to right). The core radius was held fixed in proper length at 60 pc for Halo A, 680 pc for Halo B, and 400 pc for Halo C.

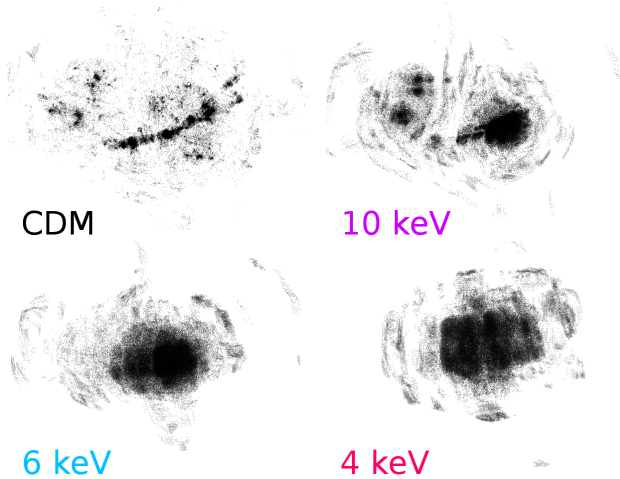


Figure 10. Positions at $a = 0.05$ of core particles in select cosmologies of the small mass scale simulations of Halo A. Images are centred on the centre of mass of core particles.

cosmologies have shown the maximum circular velocity decreases and the radius where this occurs increases for dwarf galaxy-sized haloes (Lovell et al. 2012; Anderhalden et al. 2013; Polisensky & Ricotti 2014). Figure 11 shows the circular velocity profiles of the small mass scale simulations of Halo A at the normalization time. It is clear the rearrangement of mass in the inner regions has not affected the maximum circular velocity or its location to be in disagreement with the conclusions of previous works.

It is well established that in WDM cosmologies haloes below the truncation scale form later and have lower concentrations than CDM haloes of similar size (Avila-Reese et al. 2001; Bode et al. 2001; Knebe et al. 2002). In contrast, Anderhalden & Diemand (2013) examined their three CDM microhaloes and found higher concentrations when NFW profiles were fit to the haloes in the filtered power spectrum simulations. However, they found fitting generalized profiles, where the inner slope is allowed to be a free parameter, shifted the scale radius r_s outward and reduced the concentrations.

We investigated the halo concentrations in the low resolution, large refinement volume simulations described in Section 4. These simulations were run for the small and large box sizes and 6 keV and 1.1 keV cosmologies, respectively. We fit NFW and generalized density profiles to the nine largest haloes in the refinement volume that were composed of $> 10^5$ particles and satisfied the relaxation metrics at the normalization times. We found seven of the nine haloes had greater NFW concentrations in WDM than CDM. However, six of the nine haloes had lower concentrations when generalized profiles were fit, consistent across box sizes and consistent with the microhalo results (Anderhalden & Diemand 2013; Ishiyama 2014). We found the same results when comparing the concentrations of Haloes A, B, and C at the end of the high-resolution extended simulation set. Interestingly, in the simulations with $M_f \sim 1.7M$ the NFW concentrations of Haloes B and C were less than their CDM concentrations while Halo A was greater. This is consistent with the density profiles in Figure 7 and the later formation epochs of

Haloes B and C, that enhance the filtering of substructure for a given filtering scale.

Our WDM halo profiles are similar to the profiles seen by Avila-Reese et al. (2001) and Colín et al. (2008). Colín et al. (2008) simulated five galactic-sized haloes in WDM and found profiles were steeper and denser in the inner region than the best-fitting NFW profiles. Additionally, our simulations explain a feature seen in the HDM cluster simulations of Wang & White (2009). The stacked phase space density profiles of their 20 most massive haloes show a flattening in the inner $0.05R_{vir}$ in HDM similar to the features seen in the warmest simulations of Figure 8.

Our results seem to conflict with the work of Busha et al. (2007). They evolved their CDM and WDM simulations into the future until the scale factor $a = 100$. Past the current epoch the cosmological constant quickly dominates the density of the universe ($\Omega_\Lambda \rightarrow 1$) leading to exponential expansion and the suppression of structure growth at $a \sim 3$. Thus, examining halo properties in the far future guarantees the haloes have ample time to relax into their equilibrium states. They find the average density profiles for haloes near the filtering mass are well fit by the NFW profile for $r > 0.05R_{vir}$ with only lower concentrations below the filtering mass (although the outer slope in both CDM and WDM is steeper due to the inflating universe, as noted by Ricotti 2003). However, there are two things that complicate comparison of these simulations to ours. First is the difficulty due to the different epochs the haloes are examined at. We examine our haloes shortly after the end of the fast accretion phase when the inner profile is set but the outskirts are still growing while Busha et al. examine their haloes well after all halo growth has stopped and R_{vir} has reached a maximum. The effects we see in the inner halo will therefore be at radii smaller than the convergence radius in the haloes simulated by Busha et al.. Also, they explored haloes at a larger mass scale and used a much greater filtering mass, $1.2 \times 10^{14} M_\odot$. In this work we have shown how even the density profiles of CDM haloes have a dependence on mass with smaller differences between CDM and WDM profiles for larger halo masses, for a fixed ratio of the filtering mass to halo mass.

Finally, we comment on the effects of adding thermal velocities appropriate to the adopted WDM models to the simulation particles. Thermal WDM particles decouple with a finite fine-grain phase space density that imposes an upper limit on their density, resulting in soft cores in collapsed haloes. The radius of this core depends on the mass of the WDM particle and the mass of the halo (Hogan & Dalcanton 2000). For the warmest cosmologies of Halo A the core radius is $\sim 4 \times 10^{-4} R_{vir}$ which agrees with the core sizes seen in the simulations of Macciò et al. (2012). The thermal core would be about the size of the adopted softening lengths, far below the scales where the WDM profiles deviate from the CDM profile.

7 SUMMARY

We tested the claim that the virialization process erases all information about the initial conditions and produces universal profiles in gravitationally collapsed dark matter haloes. We simulated an isolated halo with an early for-

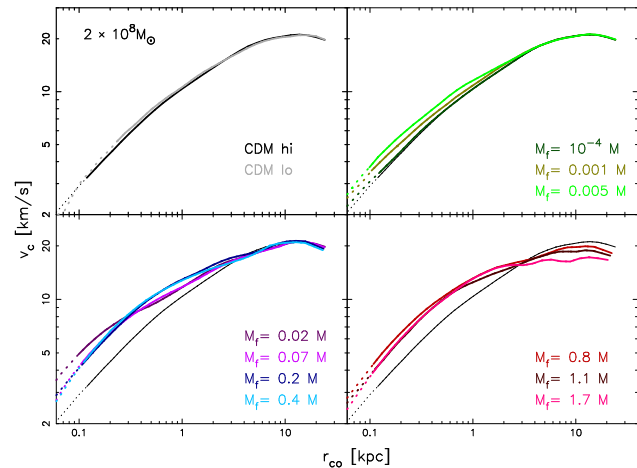


Figure 11. Circular velocity profiles of the small mass scale simulations of Halo A. The WDM profiles are grouped and plotted against the CDM profile for clarity.

matation epoch at three mass scales from $2 \times 10^8 M_\odot$ to $6 \times 10^{10} M_\odot$ in CDM and a variety of WDM cosmologies where the formation of structures below the filtering scale is suppressed. We examined when the halo was composed of $\sim 10^7$ particles at each scale and the halo was in the slow growth phase. We studied two additional haloes to account for cosmic variance. We found the haloes were changed both structurally and dynamically by the truncation in the WDM power spectra. Substructures in the mass range $10^{5-6} M_\odot$ have a detectable effect on the slope of the inner density profile in $10^{8-9} M_\odot$ haloes because when substructure on this mass scale is filtered out in the 34 keV WDM cosmology the profile visibly deviates from CDM, becoming steeper. We summarize our main findings below.

- Density profiles are steeper in WDM than CDM for haloes near the filtering scale. For $M_f < M$, the slopes approach a constant value moving from the virial radius to the inner halo, whose value is well described by the fitting formula of Ishiyama (2014). The value of the constant slope and its radial span depend on the filtering scale, moving outward and becoming steeper as the ratio of the filtering to halo mass gets larger. Our simulations also examined the regime $M_f > M$ and found the density profiles do not approach a constant asymptotic slope at intermediate radii but continue to flatten monotonically. At smaller radii, for all the masses and WDM cosmologies, the slopes do not remain at the constant value found at intermediate radii but grow shallower and become softer than CDM for $r < 0.01R_{vir}$, in agreement with halo models (Williams et al. 2004; Viñas et al. 2012).

- Particle velocity dispersions increase in the inner profiles while velocity anisotropies after virialization are largely similar across cosmologies. The changes in density and velocity dispersion create a deviation from a simple power law in the inner phase space density profiles. This deviation reaches a maximum at a radius proportional to the filtering scale.

- The core features of the profiles are set early when the halo mass growth rate $\dot{M} \sim 6 - 10$. At higher growth rates the profiles exhibit large fluctuations. After formation the core features are dynamically stable.

- The halo mass structure is rearranged in WDM compared to CDM with radii $< 0.1R_{vir}$ gaining mass at the

expense of radii $0.1 - 0.4R_{vir}$. Furthermore, the core is built up gradually in CDM from particles distributed asymmetrically in clumps about the centre of mass in contrast to WDM where the core is formed in an impulsive event from particles distributed smoothly and symmetrically. There is a correlation between the number of particles and the spin of the core with more massive cores having less spin. This argues for angular momentum as the physical mechanism responsible for the differences in profiles as seen in the models of Del Popolo (2009, 2010).

- We found a dependence on mass in the CDM profiles with larger haloes exhibiting a steeper density profile as in Ricotti (2003). The spin parameter decreases with increasing mass in agreement with the models of Del Popolo (2009) that more massive haloes have less angular momentum resulting in steeper profiles. However, the effects are much weaker than those of the truncated power spectrum. The WDM haloes had similar spins across mass scales and also had similar profiles.

Our work complements and reinforces the results of recent simulations of microhaloes near the CDM filtering scale (Ishiyama et al. 2010; Anderhalden & Diemand 2013; Ishiyama 2014) and shows that the shape of halo profiles cannot be parameterized simply by a generalized NFW or Einasto profile with a concentration or scale radius dependent on the mass or cosmology. The halo shape is more complex, with logarithmic slopes that can vary non-monotonically and with features in the profile that reflect the shape of the initial matter power spectrum. Thus, in general haloes cannot be fitted by a universal density profile. This is actually good news because it may become feasible to find fingerprints of the initial power spectrum of perturbations on galactic or sub-galactic scales in the density profiles of dark matter dominated dwarf galaxies or clusters.

ACKNOWLEDGMENTS

The simulations presented in this work were run on the DEPTHOUGHT computing cluster at the University of Maryland College Park, the Cray XE6 GARNET at the U.S. Army Engineer Research and Development Center and the SGI Ice X SPIRIT at the U.S. Air Force Research Laboratory. Basic research in astrophysics at NRL is funded by the U.S. Office of Naval Research. EP acknowledges support under the Edison Memorial Graduate Training Program at the Naval Research Laboratory. The authors acknowledge the University of Maryland supercomputing resources (<http://www.it.umd.edu/hpcc>) made available in conducting the research reported in this paper. MR's thanks the National Science Foundation and NASA for support under the grants NASA NNX10AH10G, NSF CMMI1125285 and the Theoretical and Computational Astrophysics Network (TCAN) grant AST1333514.

REFERENCES

Anderhalden D., Diemand J., 2013, JCAP, 4, 9
 Anderhalden D., Schneider A., Macciò A. V., Diemand J., Bertone G., 2013, JCAP, 3, 14

Ascasibar Y., Yepes G., Gottlöber S., Müller V., 2004, MNRAS, 352, 1109
 Austin C. G., Williams L. L. R., Barnes E. I., Babul A., Dalcanton J. J., 2005, ApJ, 634, 756
 Avila-Reese V., Colín P., Valenzuela O., D'Onghia E., Firmani C., 2001, ApJ, 559, 516
 Barnes E. I., Williams L. L. R., Babul A., Dalcanton J. J., 2006, ApJ, 643, 797
 Belokurov V., Walker M. G., Evans N. W., Faria D. C., Gilmore G., Irwin M. J., Koposov S., Mateo M., Olszewski E., Zucker D. B., 2008, ApJ, 686, L83
 Bertschinger E., 1985, ApJS, 58, 39
 Bertschinger E., 2001, ApJS, 137, 1
 Bode P., Ostriker J. P., Turok N., 2001, ApJ, 556, 93
 Bullock J. S., Kravtsov A. V., Weinberg D. H., 2001, ApJ, 548, 33
 Busha M. T., Evrard A. E., Adams F. C., 2007, ApJ, 665, 1
 Colín P., Avila-Reese V., Valenzuela O., 2000, ApJ, 542, 622
 Colín P., Valenzuela O., Avila-Reese V., 2008, ApJ, 673, 203
 Dekel A., Devor J., Hetzroni G., 2003, MNRAS, 341, 326
 Del Popolo A., 2009, ApJ, 698, 2093
 Del Popolo A., 2010, MNRAS, 408, 1808
 Diemand J., Moore B., Stadel J., 2004, MNRAS, 353, 624
 Einasto J., 1965, Trudy Astrofizicheskogo Instituta Alma-Ata, 5, 87
 Eisenstein D. J., Hu W., 1998, ApJ, 496, 605
 Gott III J. R., 1975, ApJ, 201, 296
 Graham A. W., Merritt D., Moore B., Diemand J., Terzić B., 2006, AJ, 132, 2701
 Gunn J. E., Gott III J. R., 1972, ApJ, 176, 1
 Hiotelis N., 2002, A&A, 382, 84
 Hogan C. J., Dalcanton J. J., 2000, Phys. Rev. D, 62, 063511
 Huss A., Jain B., Steinmetz M., 1999a, ApJ, 517, 64
 Huss A., Jain B., Steinmetz M., 1999b, MNRAS, 308, 1011
 Ishiyama T., 2014, ApJ, 788, 27
 Ishiyama T., Makino J., Ebisuzaki T., 2010, ApJ, 723, L195
 Jing Y. P., 2000, ApJ, 535, 30
 Jing Y. P., Suto Y., 2000, ApJ, 529, L69
 Klypin A. A., Trujillo-Gomez S., Primack J., 2011, ApJ, 740, 102
 Knebe A., Devriendt J. E. G., Mahmood A., Silk J., 2002, MNRAS, 329, 813
 Knollmann S. R., Knebe A., 2009, ApJS, 182, 608
 Lacey C., Cole S., 1993, MNRAS, 262, 627
 Lovell M. R., Eke V., Frenk C. S., Gao L., Jenkins A., Theuns T., Wang J., White S. D. M., Boyarsky A., Ruchayskiy O., 2012, MNRAS, 420, 2318
 Lu Y., Mo H. J., Katz N., Weinberg M. D., 2006, MNRAS, 368, 1931
 Ludlow A. D., Navarro J. F., Angulo R. E., Boylan-Kolchin M., Springel V., Frenk C., White S. D. M., 2014, MNRAS, 441, 378
 Ludlow A. D., Navarro J. F., Boylan-Kolchin M., Bett P. E., Angulo R. E., Li M., White S. D. M., Frenk C., Springel V., 2013, MNRAS, 432, 1103
 Ludlow A. D., Navarro J. F., Li M., Angulo R. E., Boylan-Kolchin M., Bett P. E., 2012, MNRAS, 427, 1322
 Lynden-Bell D., 1967, MNRAS, 136, 101

- Macciò A. V., Dutton A. A., van den Bosch F. C., 2008, MNRAS, 391, 1940
- Macciò A. V., Dutton A. A., van den Bosch F. C., Moore B., Potter D., Stadel J., 2007, MNRAS, 378, 55
- Macciò A. V., Paduroiu S., Anderhalden D., Schneider A., Moore B., 2012, MNRAS, 424, 1105
- Manrique A., Raig A., Salvador-Solé E., Sanchis T., Solanes J. M., 2003, ApJ, 593, 26
- Moore B., Ghigna S., Governato F., Lake G., Quinn T., Stadel J., Tozzi P., 1999, ApJ, 524, L19
- Moore B., Quinn T., Governato F., Stadel J., Lake G., 1999, MNRAS, 310, 1147
- Navarro J. F., Frenk C. S., White S. D. M., 1996, ApJ, 462, 563
- Navarro J. F., Frenk C. S., White S. D. M., 1997, ApJ, 490, 493
- Navarro J. F., Hayashi E., Power C., Jenkins A. R., Frenk C. S., White S. D. M., Springel V., Stadel J., Quinn T. R., 2004, MNRAS, 349, 1039
- Neto A. F., Gao L., Bett P., Cole S., Navarro J. F., Frenk C. S., White S. D. M., Springel V., Jenkins A., 2007, MNRAS, 381, 1450
- Nusser A., Sheth R. K., 1999, MNRAS, 303, 685
- Peebles P. J. E., 1974, ApJ, 189, L51
- Polisensky E., Ricotti M., 2011, Phys. Rev. D, 83, 043506
- Polisensky E., Ricotti M., 2014, MNRAS, 437, 2922
- Power C., Navarro J. F., Jenkins A., Frenk C. S., White S. D. M., Springel V., Stadel J., Quinn T., 2003, MNRAS, 338, 14
- Prada F., Klypin A. A., Cuesta A. J., Betancort-Rijo J. E., Primack J., 2012, MNRAS, 423, 3018
- Press W. H., Schechter P., 1974, ApJ, 187, 425
- Ricotti M., 2003, MNRAS, 344, 1237
- Ricotti M., Pontzen A., Viel M., 2007, ApJ, 663, L53
- Ricotti M., Wilkinson M. I., 2004, MNRAS, 353, 867
- Sommer-Larsen J., Dolgov A., 2001, ApJ, 551, 608
- Springel V., 2005, MNRAS, 364, 1105
- Subramanian K., Cen R., Ostriker J. P., 2000, ApJ, 538, 528
- Syer D., White S. D. M., 1998, MNRAS, 293, 337
- Taylor J. E., Navarro J. F., 2001, ApJ, 563, 483
- Viñas J., Salvador-Solé E., Manrique A., 2012, MNRAS, 424, L6
- Wang J., White S. D. M., 2007, MNRAS, 380, 93
- Wang J., White S. D. M., 2009, MNRAS, 396, 709
- Wechsler R. H., Bullock J. S., Primack J. R., Kravtsov A. V., Dekel A., 2002, ApJ, 568, 52
- White S. D. M., 1996, in Lahav O., Terlevich E., Terlevich R. J., eds, Gravitational dynamics Violent Relaxation in Hierarchical Clustering. p. 121
- Williams L. L. R., Babul A., Dalcanton J. J., 2004, ApJ, 604, 18
- Zhao D. H., Jing Y. P., Mo H. J., Börner G., 2003, ApJ, 597, L9
- Zhao D. H., Jing Y. P., Mo H. J., Börner G., 2009, ApJ, 707, 354
- Zhao D. H., Mo H. J., Jing Y. P., Börner G., 2003, MNRAS, 339, 12